International Core Journal of Engineering Volume 12 Issue 3, 2026
ISSN: 2414-1895 DOI: 10.6919/ICJE.202603_12(3).0021

Three-Dimensional Design of a Rear-Drive Self-Balancing Electric Wheelchair Chassis

Yang Gao, Aihua Tian*, Zhesheng Hou

Jilin University of Chemical Technology, Jilin, Jilin, China

*Corresponding author: Aihua Tian

Abstract

This study presents the design of a rear-drive self-balancing electric wheelchair chassis. Based on the characteristics of practical application scenarios and the requirements for medical device products, the overall structure and layout of the chassis were determined. Key components including the chassis structure, drive system, self-balancing linear actuators, and central frame were designed. The overall three-dimensional modeling and virtual assembly were carried out using the 3D modeling software SolidWorks. Mechanical analysis of the chassis frame was performed using the finite element analysis software ANSYS to optimize the structural design. Static and dynamic characteristic analyses of the chassis structure were conducted based on ANSYS. The results indicate that the chassis structure design is reasonable, with no resonance occurring during operation. Under static full-load and uniform-speed full-load conditions, the structural strength meets the design requirements for practical work. Through a combination of theoretical analysis and prototype testing, the various performance characteristics of the self-balancing wheelchair chassis system were verified. The experimental results demonstrate that the chassis possesses good motion control performance, stability, and comfort, satisfying the requirements for practical operation.

Keywords

Wheelchair; Chassis; ANSYS; Finite Element Analysis; Self-balancing.

1. Introduction

According to the data on the age composition of the national population from the Seventh National Population Census, the proportion of the population aged 60 and above in 2021 increased by as much as 5.44 percentage points compared to 2020, with a net increase of over ten million people. It is predicted that over the next twelve years, the newly added population aged 60 and above in China will equal the total accumulated over the past forty years. This data indicates that since the beginning of the 21st century, the demand for electric wheelchairs among the elderly and individuals with mobility impairments has been continuously increasing [1]. Existing traditional wheelchairs still have many shortcomings in terms of function and performance, making them unable to adapt to application scenarios in complex environments, thereby reducing the users' quality of life. In response to the current developmental challenges faced by wheelchairs, researching and developing an intelligent, automated wheelchair to enhance the performance and functionality of electric wheelchairs is of great significance for improving the user experience, enriching multi-scenario applications, and enhancing usage safety.

Currently, the functions of intelligent electric wheelchairs primarily focus on obstacle crossing, stair climbing, and multi-drive systems, with few self-balancing electric wheelchairs specifically designed for climbing stability. Focusing on the design of intelligent wheelchair chassis, Feng Changlong et al.

ISSN: 2414-1895 DOI: 10.6919/ICJE.202603_12(3).0021

[2] conducted a design analysis and application of a bionic wheel-leg stair-climbing chassis structure, proposing the use of bionic principles to optimize the structural design of the wheelchair chassis and improve its adaptability on complex terrain. Liu Cheng et al. [3] researched a reconfigurable wheel-track composite propulsion mechanism for ground mobile platforms, suggesting that reconfigurable design can enhance the flexibility and adaptability of the wheelchair chassis. Wang Zhanli et al. [4] designed a climbing mechanism for a crank star-wheel stair-climbing wheelchair, providing technical support for improving the stability and reliability of wheelchairs during stair climbing. In summary, the ability of existing intelligent electric wheelchairs to overcome obstacles and climb stairs mainly relies on reconfiguring the wheelchair's wheel structure to achieve the desired effect. These designs are tailored to specific operational scenarios and have relatively monotonous functions. Furthermore, vibrations and noise generated during operation can affect the user's experience to some extent.

Electric wheelchairs currently available on the market primarily use a rear-mounted single motor as the power source, supplemented by front casters for turning. Although this offers a considerable improvement in user experience and travel efficiency compared to traditional manual wheelchairs, problems such as insufficient power, less responsive turning, and overall instability and a tendency to tip over on inclines still exist. This paper proposes a rear-wheel dual-motor self-balancing electric wheelchair chassis, designed to achieve a self-balancing function, based on the daily usage requirements of actual electric wheelchairs. The chassis structure and key components are designed. The various performance characteristics of the wheelchair chassis are verified and improved through theoretical analysis, simulation, and prototype testing, ensuring the daily usability of the self-balancing electric wheelchair.

2. Overall Scheme Design

2.1 Design Objectives and Overall Structure

The main operating scenarios for the rear-wheel dual-motor self-balancing electric wheelchair chassis are on slopes ranging from -15° to +15°. Based on the characteristics of these practical scenarios and the needs of users, the chassis design must satisfy the following:

(1) It must be capable of ascending and descending slopes between -15° and +15°, during which the seat must remain level overall. The deviation between the seat and the horizontal plane should be controlled within ±0.5°, ensuring that the driver does not perceive changes in the slope angle.

(2) It must exhibit good trafficability and driving stability on complex surfaces. The firmware strength and metal fatigue during continuous ascending and descending must remain within allowable error ranges.

(3) The chassis structure should be compact and reasonable, with strength and rigidity that meet daily driving requirements, ensuring driving stability and safety.

(4) It must provide sufficient power output and a range of approximately 30 km to meet the requirements for long-duration wheelchair use. The turning radius should be within 1.5 m, and the braking must be responsive and reliable.

The self-balancing electric wheelchair is primarily composed of the chassis, a self-balancing pressure rod adjustment system, the seat, a manual control joystick, a display screen, and leg rests.

As shown in Figure 1, the batteries and drive components are centrally installed in the chassis. The chassis houses the central frame, a seat support plate, the battery pack, and dual motors. A pair of drive wheels and a pair of driven wheels are installed on the left and right sides to provide mobility and steering functions. The battery pack consists of three 12V lead-acid batteries, with two positioned on the left and right sides of the vehicle body and the third placed at the bottom of the seat pan.

ISSN: 2414-1895 DOI: 10.6919/ICJE.202603_12(3).0021

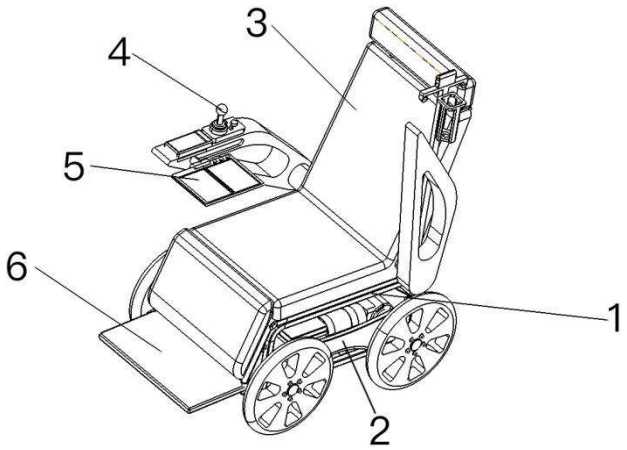

1. Chassis; 2. Self-balancing Pressure Rod Adjustment System; 3. Seat;
4. Manual Control Joystick; 5. Display Screen; 6. Leg Rests

Figure 1. Overall structure of the self-balancing electric wheelchair

2.2 Working Principle

The power source for the rear-wheel dual-motor self-balancing electric wheelchair chassis is three lead-acid batteries. Two of the 12V lead-acid batteries are connected in series to form a 24V power supply, which provides power to the 1.2kW drive motors on the left and right sides, as well as to the linear actuators for balancing. The other 12V lead-acid battery powers the slope display, the manual control joystick, and the emergency braking system. When the wheelchair's electronic control switch is activated, the MPU6050 gyroscope in the self-balancing system collects acceleration and angular velocity data, converting it into slope information. When the slope reaches a preset critical value, an early warning signal is output, alerting the user that they are entering an uphill/downhill state. The system substitutes the slope value into a dynamic calculation model to determine the minimum output power required from the motors and electric linear actuators. Based on the calculation results, the control module synchronously adjusts the motor speed and torque to provide climbing power. Simultaneously, it coordinates the length adjustment of the four electric linear actuators based on the principle of a parallel mechanism, dynamically compensating for the body's tilt. This maintains the horizontal stability of the wheelchair platform, ensuring ride comfort and the safe operation of the equipment.The main technical parameters of the self-balancing electric wheelchair are shown in Table 1:

Table 1. Main Technical Parameters of the Self-Balancing Electric Wheelchair

Serial number	Name of index	Parameter	Serial number	Name of index	Parameter
1	Dimensions (cm)	150×120×120	5	Maximum Range (km)	30
2	Motor Drive Power (kW)	1.2	6	Maximum Speed (km/h)	20
3	Maximum Climbing Angle (°)	15	7	Minimum Turning Radius (m)	1.5
4	Maximum Descending Angle (°)	15	8	Load Capacity (kg)	200

ISSN: 2414-1895 DOI: 10.6919/ICJE.202603_12(3).0021

3. Design of Key Components

3.1 Design of the Drive System

The driving resistance encountered by the self-balancing electric wheelchair during daily operation includes rolling resistance, grade resistance, acceleration resistance, and air resistance. The primary working resistance is the grade resistance. Assuming the self-balancing electric wheelchair travels at a uniform low speed, the acceleration resistance and air resistance can be neglected. The driving resistance can be expressed as:

$$\begin{cases} f=f_1+f_2+f_3 \\ f_2=G\cdot \sin\alpha \\ f_1=G\cdot\sigma\cdot \cos\alpha \end{cases} \tag{1}$$

In the formula: f is the driving resistance (N);

In the formula: f is the driving resistance (N); f_1, f_2, and f_3 are the rolling resistance (N), grade resistance (N), and working resistance (N), respectively; G is the gravity force of the self-balancing electric wheelchair (N); α is the slope angle (°); σ is the rolling resistance coefficient.

The power of a single drive motor can be calculated using Equation (2):

$$P=\frac{f\cdot v}{i\cdot\eta} \tag{2}$$

In the formula:

P is the power of a single drive motor (W);

v is the operating speed (m/s);

i is the number of drive motors;

η is the mechanical transmission efficiency. According to actual test results, the working resistance of the self-balancing system is 20 N,Working resistance f_3 = 20 N.

The self-balancing electric wheelchair's own gravity G =4000 N,Slope angle α=15°.Rolling resistance coefficient σ=0.1.Substituting the above values into Equation (1), the calculated driving resistance f=1108.32 N.Taking the operating speed v=2m/s, mechanical transmission efficiencyη= 0.95, and i = 2, and substituting into Equation (3), the power of a single drive motor is calculated as P = 1.16 kW.

Therefore, a drive motor with a rated power of 1.2 kW, rated voltage of 24 V, and rated speed of 3000 r/min is selected.

When the chassis is traveling on a road surface, the contact friction between the wheel tires and the ground provides the forward driving force for the whole machine. During travel, the load causes slight subsidence of the tires, which leads to energy loss. Assuming the road surface is a rigid body, the expression for the wheel driving resistance can be derived based on the Bekker pressure-sinkage formula as follows:

$$f=\frac{\left(3\frac{F_n}{\sqrt{\varphi}}\right)^{\frac{2n+2}{2n+1}}}{(3-n)^{\frac{2n+2}{2n+1}}\cdot(1+n)\cdot\left(K_c+xK_\varphi\right)^{\frac{1}{2n+1}}} \tag{3}$$

ISSN: 2414-1895 DOI: 10.6919/ICJE.202603_12(3).0021

Where:

F_n is the support force from the ground to the wheel (N);

x is the wheel width (mm);

φ is the wheel diameter (mm);

Kc is the cohesive modulus;

Kφ is the friction modulus;

n is the sinkage index.

According to Equation (3), when other parameters are constant, the driving resistance decreases with the increase in wheel width and diameter. Considering factors such as the chassis wheelbase, overall length, and minimum ground clearance, and to avoid structural damage under load, the final selected wheel specifications are a height of 500 mm, width of 100 mm, and a maximum load capacity of 200 kg.

3.2 Design of the Central Frame

The central frame is a key component for the wheelchair to achieve posture changes, undertaking the important tasks of connecting various motion mechanisms and transmitting loads. Since most of the user's body weight will ultimately act on this frame, especially with the most concentrated force in the seated position, the strength and stiffness of the central frame must be ensured. At the same time, considering the overall weight reduction requirements of the wheelchair, as well as the potential oxidation and corrosion issues in daily use, the material selection also requires comprehensive trade-offs.

Based on the above considerations, 6061 aluminum alloy was selected as the processing material for the central frame. This material is relatively mature in practical engineering applications. It possesses good mechanical properties to meet load-bearing requirements, while its low density helps control the overall weight of the machine and reduces the driving burden on the electric linear actuators. Furthermore, 6061 aluminum alloy offers good corrosion resistance and requires simple surface treatment processes, making it adaptable to daily use environments and meeting the basic requirements of durability and hygiene for medical devices.

3.3 Static Characteristic Analysis of the Central Frame

Analysis of the static and dynamic characteristics of the central frame was conducted based on ANSYS to verify the rationality of the central frame structural design. The central frame model was imported into Workbench 2021 R1 software. The material for the central frame was set as 6061 aluminum alloy, with a density of 2700 kg/m³, Young's modulus of 71 GPa, and Poisson's ratio of 0.33. To improve simulation accuracy and computational speed, the central frame model was simplified as follows: ① some mounting holes were ignored, ② chamfers and fillets were simplified to right angles, and ③ the influence of welding on the material properties of the central frame was not considered. The material parameters are shown in table 2 below. After simplification by removing redundant parts, the modified overall mass is 4.67 kg.

Table 2. Parameters of 6061 aluminum alloy for the central frame

	Property	Value	Unit
2	Density	2770	kg m^-3
3	Isotropic Secant Coefficient of Thermal Expansion		
6	Isotropic Elasticity		
7	Derive from	Young's Modulus and Poisson's...	
8	Young's Modulus	7.1E+10	Pa
9	Poisson's Ratio	0.33	
10	Bulk Modulus	6.9608E+10	Pa
11	Shear Modulus	2.6692E+10	Pa
12	Alternating Stress R-Ratio	Tabular	
16	Tensile Yield Strength	280	MPa
17	Compressive Yield Strength	280	MPa
18	Tensile Ultimate Strength	310	MPa
19	Compressive Ultimate Strength	0	Pa

ISSN: 2414-1895 DOI: 10.6919/ICJE.202603_12(3).0021

As shown in Figure 2, the temperature was selected as room temperature conditions. For meshing, 146,060 nodes were selected to generate 78,898 mesh elements. The inner annular surface of the cross hinge joint and the bottom boss surface were designated as fixed supports.

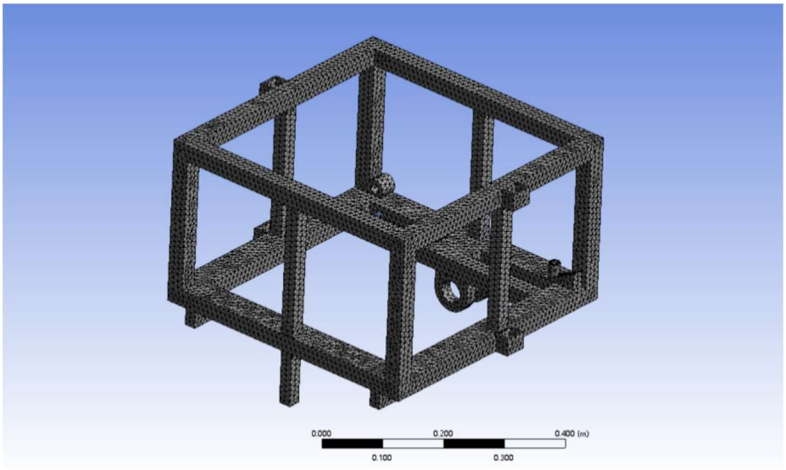

Figure 2. Mesh generation display

A standard Earth gravity was applied in the -Z axis direction. Simultaneously, a bearing capacity of 2000 N was applied as a uniformly distributed load on the central frame in the Z-axis direction. The total deformation, equivalent elastic strain, and von Mises equivalent stress were solved, and the results are shown in Figure 3. Comparing the results, if they are less than the allowable deformation values, the design meets the standard.

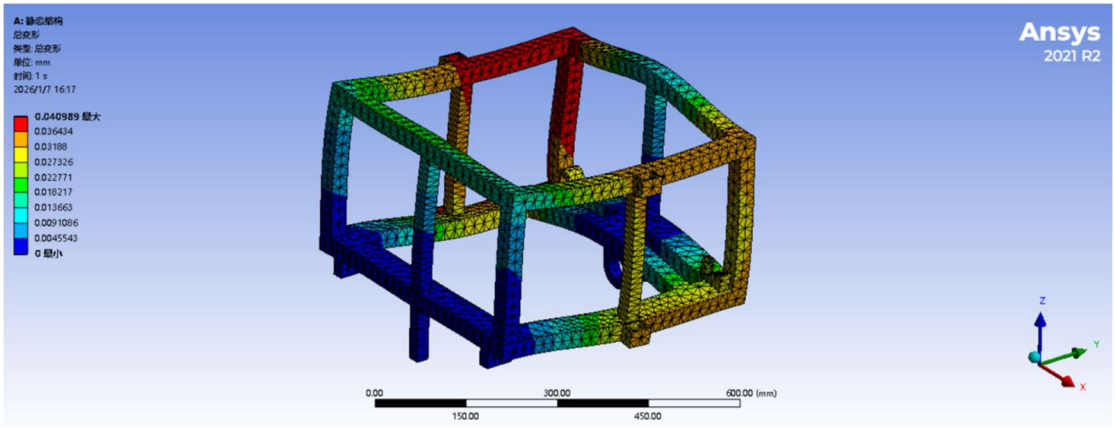

(a) Full-Load Total Deformation

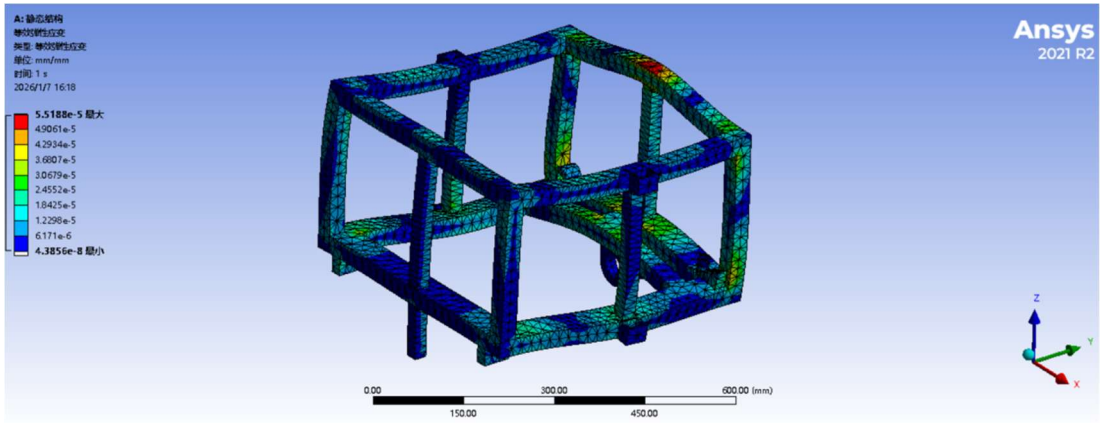

(b) Full-Load Equivalent Elastic Strain

ISSN: 2414-1895 DOI: 10.6919/ICJE.202603_12(3).0021

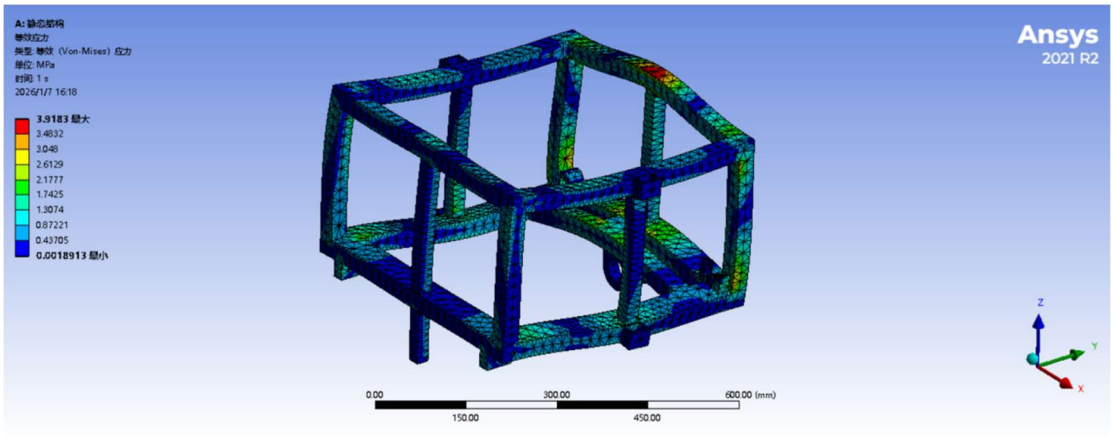

(c) Full-Load von Mises Equivalent Stress

Figure 3. Total deformation, equivalent elastic strain, and von Mises equivalent stress of the central frame under full load condition

From Figures (a) and (b), it can be seen that when subjected to a full load of 2000 N as a uniformly distributed load, the maximum deformation of the central frame is 0.04 mm, and the maximum strain value of the central frame is 0.00055 mm. When the material exceeds elastic deformation and undergoes plastic deformation, the central frame component will lose its original performance. For this material at room temperature, the elastic deformation limit and the allowable maximum strain value are 0.4 mm and 0.00157 mm, respectively. The data indicates that under full load conditions, the deformation of the central frame is far less than the elastic limit and does not exceed the allowable maximum strain value, placing it within a reasonable design range.

From Figure (c), it can be seen that the von Mises equivalent stress under full load conditions is 3.9183 MPa. Since the central frame is made of aluminum alloy, its mass is only 30% of a steel structure. Furthermore, by adding support columns on the four sides of the frame, the maximum stress was reduced from 15.51 MPa to 3.9183 MPa, making the structure more reliable. The ultimate von Mises equivalent stress for this aluminum alloy under standard room temperature and static loading conditions is 276 MPa, which is significantly higher than the experimental result.

According to the static analysis results, no obvious stress concentration points were found that would lead to overall collapse. Although there are relatively larger stress and deformation values locally on the central frame, the stresses in all areas are below the material's yield strength, and the deformation is minimal relative to the overall dimensions. This indicates that the structural design of the central frame is reasonable, and its strength can meet the requirements for normal operation under full load conditions. The upper part of the cross hinge joint of the central frame is the reserved installation position for the seat base plate. Observing the stress cloud diagram, it is found that this area experiences the greatest stress and deformation, but it remains within the reasonable design range. By installing the seat base plate, the impact of this local deformation on the overall central frame can be reduced, thereby enhancing the structural strength and reliability.

3.4 Design of the Self-balancing Linear Actuators

The self-balancing linear actuator system consists of four electric linear actuators and serves as the executive component for adjusting the wheelchair's posture and achieving automatic leveling. The bottoms of the four actuators are connected to the wheelchair base via hinges, and their tops are fixed to the four corners of the central frame, forming a four-point support structure. This arrangement allows the actuators to operate both independently and cooperatively, thereby enabling adjustment of the spatial posture of the central frame.

The connection between the actuators and the base uses a hinge form. The hinge axes are arranged differently according to the actuator positions: the hinge axes for the left and right actuators are

ISSN: 2414-1895 DOI: 10.6919/ICJE.202603_12(3).0021

parallel to the length direction of the wheelchair, while the hinge axis for the rear actuators is parallel to the width direction of the wheelchair. The hinged connection allows the actuators to undergo angular deflection around the axis during extension and retraction, adapting to changes in the angle between the actuator and the base, and preventing structural jamming caused by rigid connections.

The head of each actuator is connected to the central frame via a bearing. The connection axes for the left and right actuators are parallel to the width direction of the wheelchair, while the connection axis for the rear actuator is parallel to the length direction. The bearing connection compensates for minor angular deviations that may occur during actuator extension and retraction, resulting in more uniform force distribution on the actuators and smoother movement.

The four actuators share an identical structure, are driven by DC motors, and provide real-time feedback on the extension length to the control system for closed-loop regulation. When the gyroscope installed on the wheelchair body detects a tilt, the control system calculates the required target length for each actuator based on the tilt angle and drives the actuators to act, restoring the central frame to a level position. The operation of the electric linear actuator structure is shown in Figure 4.

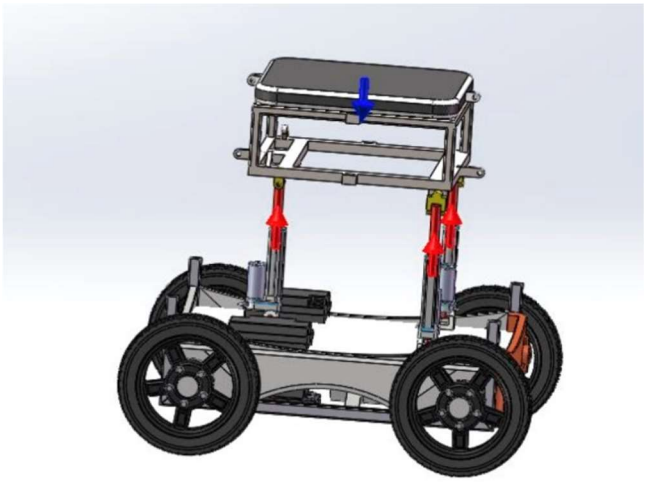

Figure 4. Electric linear actuator structure operation diagram

4. Dynamic Simulation Analysis

4.1 Experimental Component Parameters

In this design, during actual operation, the dynamic structural changes are primarily concentrated in the chassis structure parts. To ensure normal operation, the operational condition of the chassis under dynamic situations requires simulation experiments. The structure and mass distribution of the chassis affect the reliability of the whole machine's operation. The main structure of the chassis is designed as a frame-type structure. Considering both strength and lightweight requirements comprehensively, the main body of the chassis structure is welded and formed using 6061 aluminum alloy square tubes with a cross-sectional dimension of 50 mm × 50 mm × 3 mm. Compared to pure aluminum and 6063 alloy, this material offers better workability, strength, and corrosion resistance. The electric linear actuators are installed at the four corners of the central frame respectively to ensure vector balance during angle adjustment, thereby maintaining stability throughout the balancing process. Simultaneously, battery compartments are provided on the left and right sides of the chassis to balance the mass distribution of the batteries. To enhance the structural strength of the chassis, reinforcing tubes are installed between the two layers of the central frame, and angled fixing brackets are welded in place. After these improvements and optimizations, its dynamic performance was tested, and the data were analyzed.

ISSN: 2414-1895 DOI: 10.6919/ICJE.202603_12(3).0021

4.2 Simulation and Optimization Design

The performance of the self-balancing electric wheelchair is susceptible to vibrations. As the pathway for vibration transmission, the dynamic characteristics of the chassis structural components directly affect the stability of the self-balancing system. Analyzing the natural frequencies and mode shapes of the chassis can determine whether resonance occurs and indirectly assess the impact of the chassis's dynamic characteristics on the self-balancing system. Modal analysis is therefore essential for studying the mechanical structure's dynamic characteristics.

According to modal analysis theory[13], the modal dynamics equation of an object can be expressed as follows:

$$[M](\ddot{x}) + [C](\dot{x}) + [K](x) = \{F(t)\} \tag{4}$$

Where:

$[M]$ -Mass matrix;

$[C]$ - Damping matrix;

$[K]$ - Stiffness matrix;

$\{x\}$ -- Node displacement vector;

$\{\dot{x}\}$ -- Node velocity vector;

$\{\ddot{x}\}$ -- Node acceleration vector;

$\{F(t)\}$ --Time-varying node load.

To simulate the state of the chassis under actual working conditions, the model was analyzed and simplified by omitting some non-critical components, and a fixed support constraint was applied to the bottom of the central frame. Based on the Modal module of the ANSYS Workbench software, a modal analysis was performed on the power chassis structure. The modal frequencies and structural deformation for the first 6 orders of the chassis structure were obtained. Simulation was conducted within the software according to the relevant formulas to generate data. The results of the data analysis are shown in Figure 5.

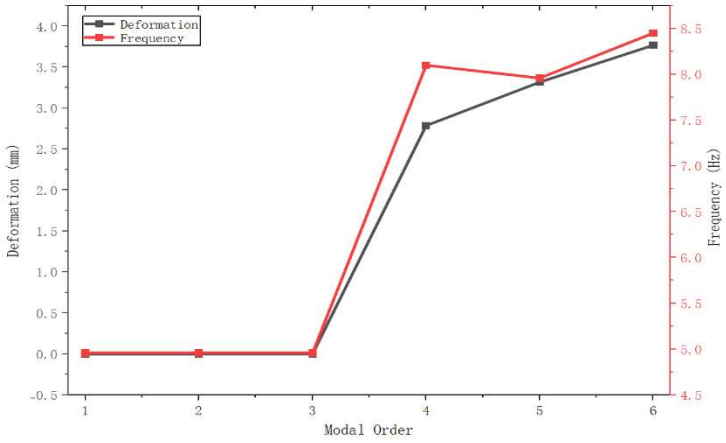

Figure 5. First 6 orders modal analysis results

The results of the initial modal analysis on the chassis structure show that as the modal order increases, both the natural frequency and the relative deformation of the structure exhibit an increasing trend. However, the natural frequencies of the first to third order modes are relatively low, falling precisely

ISSN: 2414-1895 DOI: 10.6919/ICJE.202603_12(3).0021

within the excitation frequency range (0-10 Hz) of daily operation. This makes the chassis susceptible to resonance during operation, affecting running smoothness and structural lifespan. Structural optimization was carried out on the chassis components. The main measures included adding support blocks at key locations and introducing fixed support constraints to the bearing bases to enhance the overall stiffness. After optimization, a modal simulation analysis was performed again, and the results obtained are shown in Figure 6.

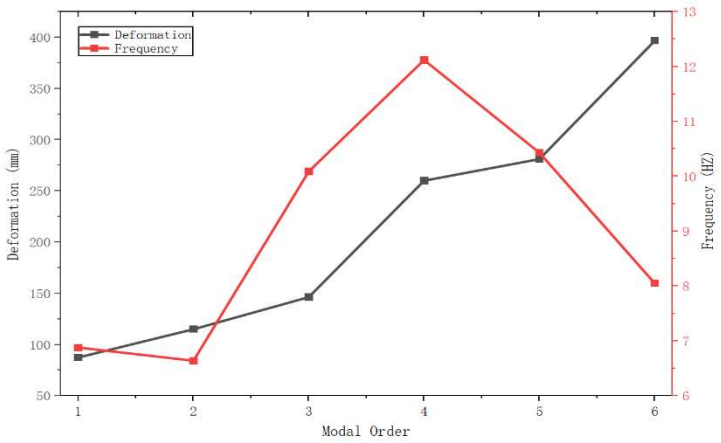

Figure 6. First 6 orders modal analysis results after optimization

From the modal analysis results, it can be seen that as the modal order increases, the deformation of the optimized chassis structure has increased compared to that before optimization. Considering the clearance fits present in the actual assembly, these deformation values serve only as a relative reference. The analysis data indicates that the maximum deformation is within the design allowable range of 0-20 mm, satisfying the stiffness requirements. A key observation is that the natural frequencies of all orders are higher than the excitation frequency range encountered in daily operation. This demonstrates that the structure will not experience resonance during operation, and its dynamic characteristics meet the usage requirements. Comparing the data before and after optimization, it is evident that the natural frequencies of each order have been significantly increased after optimization, effectively avoiding the excitation frequency range of daily operation, and the risk of resonance has been mitigated.

4.3 Dynamic Characteristic Analysis

A constrained modal analysis was performed on the chassis structure by simplifying the model and omitting unnecessary detachable parts. The Modal module in ANSYS Workbench software was used to conduct a modal analysis on the power chassis structure, obtaining the natural frequencies and vibration modes for the first six orders of the chassis structure. The natural frequencies from the first six orders of modal analysis for the chassis structure are shown in Table 3, and the corresponding vibration mode shapes for the first six orders of modal analysis frequencies of the chassis structure are shown in Figure 7.

Table 3. Natural Frequencies of the First 6 Modes in Modal Analysis

Mode	NaturalFrequency(Hz)	Mode	NaturalFrequency(Hz)
1	93.96	4	280.29
2	121.42	5	293.94
3	155.76	6	414.03

ISSN: 2414-1895 DOI: 10.6919/ICJE.202603_12(3).0021

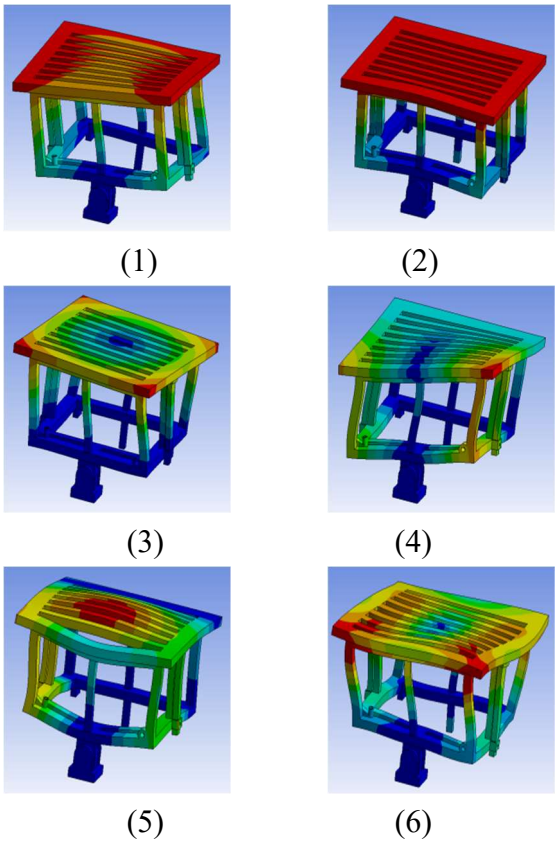

Figure 7. First 6 orders modal vibration mode shapes of the chassis structure

Compared to higher-order vibration modes, lower-order modes have a greater impact on the dynamic characteristics of the chassis structure components. From Table 2, it can be seen that the first-order natural frequency of the chassis structure is 93.96 Hz. Figure 7 shows that the maximum deformation is 6.4159 mm. According to the literature [5-6], research on the optimized design of wheelchair chassis structures based on behavioral analysis indicates that the excitation frequency during terrain undulations is between 0-20 Hz, while the excitation frequency during daily operation is between 0-10 Hz. This range of external excitation frequencies indicates that the design of the chassis structure components can effectively avoid resonance. From the distribution of the vibration modes, it can be seen that the first three orders of vibration modes of the chassis structure are mainly concentrated in the area connecting the seat base plate and the central frame (the isolation plate), which may intensify vibration transmission to the seat. It should be noted that to simplify the calculation model in this simulation analysis, the isolation plate and the surrounding structure were set as an integrated fixed connection, and were assumed to be in a tight fit state by default. However, under actual working conditions, there is a clearance fit between the isolation plate and the adjacent frame. The deformation and compression effects generated by the vibration of the lower part of the frame are alleviated to a certain extent due to the existence of this clearance, resulting in actual deformation being less than the simulation results. Moreover, this deformation does not exceed the allowable range of the isolation plate material, and the overall strength meets the design requirements. Although existing research has shown that the vibration transmission in this area has little impact on stability due to the relatively high resonance frequency, increasing the stiffness of this part could further reduce the adverse effects of vibration.

5. Conclusion

This paper addresses the issue that existing electric wheelchairs cannot maintain balance when coping with complex road conditions, such as uphill slopes, by designing a rear-wheel dual-motor self-balancing electric wheelchair chassis system.

ISSN: 2414-1895 DOI: 10.6919/ICJE.202603_12(3).0021

(1) The overall scheme of the wheelchair was designed, determining the overall layout of the chassis and the structural design of key components such as the drive system, central frame, and self-balancing linear actuators. The chassis adopts a rear-wheel dual-motor structure coordinated with four sets of self-balancing linear actuators. The bottom of each actuator is connected to the base via a hinge, and the top is fixed to the four corners of the central frame via bearings. The hinge axes are arranged according to the actuator positions, providing installation space for multi-axis adjustment.

(2) Structural design and static analysis of key components were carried out to address the issues of drive system power matching and central frame lightweighting. Based on driving resistance calculations, a 1.2 kW DC motor was selected for the drive system, meeting the requirements for climbing and range.

(3) The central frame is made of 6061 aluminum alloy, which ensures strength while reducing the overall weight. Support columns were added to the four sides of the frame, reducing the maximum stress from 15.51 MPa to 3.92 MPa. Static analysis results show that under full load conditions, the maximum deformation of the central frame is 0.04 mm and the maximum equivalent stress is 3.92 MPa, both far below the material's allowable values, verifying that the structural strength and stiffness meet the usage requirements.

(4) Modal analysis was performed using the Modal module in ANSYS Workbench software to study and optimize the dynamic characteristics of the chassis structure. To address the problem of low-order frequencies being too low due to insufficient initial support, support blocks were added at key positions on the chassis to enhance local support, and fixed support constraints were introduced to the bearing bases to improve the boundary conditions. This solved the issue where the first three natural frequencies in the initial design fell within the 0-10 Hz daily operation excitation range, making the structure prone to resonance. The dynamic characteristic analysis of the components showed that the low-order natural frequency is 93.96 Hz, which is higher than the daily operation excitation frequency range, effectively avoiding resonance. The first three vibration modes are mainly concentrated in the connection area between the seat base plate and the central frame. Although this may have some impact on vibration transmission, the natural frequency in this area is relatively high, so its influence on overall stability is limited. To simplify calculations in the simulation, the isolation plate was assumed to be in a tight fit, whereas actual assembly involves clearances that can alleviate the compression effect during frame vibration. Consequently, the actual deformation is less than the simulation results and does not exceed the material's allowable range, confirming that the overall strength meets the design requirements.

References

[1] Yuan Kui. Research Status and Trends of Intelligent Wheelchairs [J]. China Medical Device Information, 2009, 15(01): 6+33. DOI: 10.15971/j.cnki.cmdi.2009.01.023.

[2] Feng, C. L., Xing, Z. G., & Cheng, J. Design Analysis and Application of Bionic Wheel-leg Stair-climbing Chassis Structure [J]. Automation & Instrumentation, 2023, 38(7): 105-109.

[3] Liu, C., Wang, J. X., & Liu, J. F. Research Status and Prospect of Reconfigurable Wheel-track Composite Propulsion Mechanism for Ground Mobile Platforms [J]. Transactions of Beijing Institute of Technology, 2024-02-29.

[4] Wang, Z. L., Zhao, D. C., & Chen, Y. W. Design of Climbing Mechanism for Crank Star-wheel Stair-climbing Wheelchair [J]. Journal of Changchun University of Technology (Natural Science Edition), 2011, 32(2): 105-108.

[5] Zhai C, Long J, Taylor R, et al. Field scale row unit vibration affecting planting quality[J]. Precision Agriculture, 2020, 21: 589-602.

[6] MAO Jiawen, ZHOU Jun, LIANG Yangyang. Research on sliding mode control of slip rate for electric high-clearance vehicle[J]. Journal of China Agricultural University, 2017, 22(2): 129-134.